

Solid Element with Four-Point Integration in Plane for Bulk Forming

Ting Du¹, J. P. Xu¹, Y.Q. Liu² and Z. B. Zhang¹

Abstract: An eight-node hexahedral element with four-point quadrature in plane is developed using the assumed strain method, which can eliminate volumetric locking of incompressible material and absence of the portion of shear velocity strain related with hourglass mode to suppress hourglass mode and shear locking. In this approach, the radial return algorithm is adopted for more precise calculation of internal forces, stress and strain. In addition, a co-rotational coordinates system is established to make bending simulation much more effective, and the system is applicable to arbitrary 3D anisotropic yield criteria. A large elastic-plastic deformation of unconstrained thick plate bending example is then carried out with the comparison between ASQBI and ADS solid element. Numerical results of thick metal plate ironing and cylindrical piece embossing are remarkably identical to experimental results and less computation (only one hours is needed using new element in this examples while 5.5 hours using DEFORM 3D software) and higher accuracy are obtained using this new solid element by comparing with DEFORM 3D's result, which meets the demand of Shenyang Mint.

Keywords: Four-point integration; Hexahedral element; Volumetric locking; Shear locking; Hourglass mode; Bulk forming.

1 Introduction

In the late 1970s, Kosloff and Frazier (1978) developed the quadrilateral and hexahedral element based on one-point integration and hourglass control, but both of them failed in passing the patch test [Strang G(1972)]. Since 1980s, more effective reduced integration (RI) methods have emerged.

¹ State Key Laboratory of Material Processing and Die & Mould Technology, Huazhong University of Science & Technology, Wuhan Hubei 430074

² Corresponding author at: State Key Laboratory of Material Processing and Die & Mould Technology, Huazhong University of Science & Technology, 1037 Luoyu Road, Wuhan Hubei 430074, PR China. Tel.: +86 27 87558193; fax: +86 27 87554405. Email: fastamp@vip.sina.com

Firstly, Flanagan and Belytschko (1981) proposed two types of hourglass control schemes for both 2D and 3D problems: viscous and elastic, however they required user-defined parameters to control hourglass force. Belytschko et al. (1984) presented an updated hourglass control to eliminate rank deficiency of stiffness matrix, and the constructed hourglass shape vectors satisfied the consistency conditions to pass patch test. Liu et al. (1985) expanded B matrix in a Taylor series about the element centre up to bilinear terms to get six gradient sub-matrices, and then obtain six hourglass forces in terms of general three-dimensional constructive law. Koh and Kikuchi (1987) employed DRI (Directional Reduced Integration) method along one or two referential coordinate directions to stabilize mainly 2D element without locking problems. Belytschko and Binderman (1993) developed one-point integration solid element with hourglass control and four-point integration without hourglass control, entitled the ASQBI or ADS element. Only the non-constant part of standard strain field was projected to an assumed strain field, thus the volumetric locking of incompressible materials, shear locking and hourglass modes in thin plate were removed successfully. Using B-matrix method in reference [see Liu, Ong and Uras (1985)], Liu et al. (1994) adopted strain gradient sub-matrices related to shear strain terms in co-rotational coordinate system to eliminate shear locking, and then developed NUHEXIN-4 solid element with four-point integration. On the basis of Liu's method [Liu, Hu and Belytschko (1994)], stress and strain were expanded in a Taylor series about the element centre up to bilinear terms, and the constant part of stress was used to calculate internal force and non-constant part, which could be obtained by simplifying constructive matrix and corresponding strain, to calculate hourglass force. Thus, the locking problems were controlled effectively in reference [Hu and Nagy(1997); Filho and Awruch(2004)]. During the past decade, many practical one-point or multiple-points integration solid-shell and solid elements have been presented [Lee, Cho, Lee (2002); Basar and Kintzel (2003); Gato, and Shie (2008); G. M. Kulikov1 and S. V. Plotnikova (2008); Cui, Liu (2008)]. One-point integration solid element with hourglass control, named Jet3D element by Li and Cescotto (1997), could be applied in large deformation nonlinear elastic-plastic problems. In their work, rank sufficiency of stiffness matrix made the element stable, assumed strain method made the element isochoric everywhere to remove volumetric locking, and setting some shear parameters automatically linked with the studied structural dimension effectively avoided shear locking. Liu, Guo and Tang (1998) proposed HEXDS solid element for large deformation nonlinear elastic-plastic problems by adding return mapping algorithm in the previous NUHEXIN-4 solid element for updating stress and strain. Wang and Wagoner (2005) presented WW3D solid element for large deformation nonlinear problems, which was characterized by assumed strain method for avoiding volumetric locking in nearly incompressible or incompressible materials, ab-

sent of strain terms corresponding with shear locking and hourglass modes and FI method. Constructing new stability matrix based on Hu-Washizu variation principle, Fredriksson and Ottosen (2007) discussed the value of E_h matrix of regular and irregular element in details. In recent years, a new class of numerical approaches known commonly as meshfree methods have been developed to completely avoid different locking phenomena encountered in Finite Element Method. Atluri and his colleagues [Atluri and Zhu(1998); Atluri and Shen (2002); Atluri (2004); S. N. Atluri, Z. D. Han and A. M. Rajendran (2004); Z. D. Han, A. M. Rajendran and S.N. Atluri(2005); S. N. Atluri, H. T. Liu and Z. D. Han.(2006)] proposed a general framework for developing the well-known Meshless Local Petrov-Galerkin (MLPG) approach, which is a truly meshless method without under-integration and hour-glass control and provides flexibility in choosing the local weak forms, the trial functions, and the independent test functions for solving systems of partial differential equations.

Based on the WW3D element, a new solid element is formulated in the present paper, which makes use of four-point integration in plane, return mapping algorithm and adaptive mesh refine technology. This element inherits the property of WW3D element, such as no volumetric locking, shear locking and spurious modes, and decreases CPU time by fifty percent. Simulation examples of thick plate bending, thick metal plate ironing and cylindrical piece embossing are presented in the third section.

2 Four-point integration solid element in plane

2.1 Shape function of hexahedral element

Solid element in referential coordinate system is shown in Fig. 1 with eight nodes and three translation degrees exclusion of rotation degrees of freedom for each node. ξ , η and ζ are respectively three axes of the referential coordinate system, the shape function of which are expressed as the spatial coordinates x_i in element are approximated in terms of nodal coordinates x_j^i

$$N_j = (1 + \xi_j \xi)(1 + \eta_j \eta)(1 + \zeta_j \zeta)/8 \quad j = 1, 2, \dots, 8 \quad (1)$$

Eq. (1) is expanded as:

$$N_j = [1 + \xi_j \xi + \eta_j \eta + \zeta_j \zeta + (\eta_j \zeta_j) \eta \zeta + (\xi_j \zeta_j) \xi \zeta + (\xi_j \eta_j) \xi \eta + (\xi_j \eta_j \zeta_j) \xi \eta \zeta]/8 \quad (2)$$

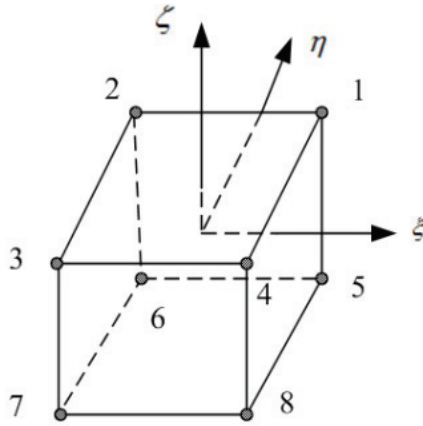


Figure 1: Solid element in referential coordinate system

Spatial coordinate of an arbitrary point in element x_i is interpolated by

$$xi = \sum_{j=1}^8 N_j X_{ij} = (S^T + l_1^T \xi + l_2^T \eta + l_3^T \zeta + m_1^T \eta \zeta + m_2^T \xi \zeta + m_3^T \xi \eta + m_4^T \xi \eta \zeta) X_i / 8$$

$$i = 1, 2, 3 \quad (3)$$

Isoperimetric element is used in this program, so displacements of an arbitrary point in element can be interpolated by

$$ui = \sum_{j=1}^8 N_j U_{ij} = (S^T + l_1^T \xi + l_2^T \eta + l_3^T \zeta + m_1^T \eta \zeta + m_2^T \xi \zeta + m_3^T \xi \eta + m_4^T \xi \eta \zeta) U_i / 8$$

$$= (U_i^0 + U_i^{l_1} \xi + U_i^{l_2} \eta + U_i^{l_3} \zeta + U_i^{m_1} \eta \zeta + U_i^{m_2} \xi \zeta + U_i^{m_3} \xi \eta + U_i^{m_4} \xi \eta \zeta) / 8 \quad i = 1, 2, 3 \quad (4)$$

where

$$S^T = (1, 1, 1, 1, 1, 1, 1, 1); \quad l_1^T = (1, -1, -1, 1, 1, -1, -1, 1);$$

$$l_2^T = (1, 1, -1, -1, 1, 1, -1, -1); \quad l_3^T = (1, 1, 1, 1, -1, -1, -1, -1);$$

$$m_1^T = (1, 1, -1, -1, -1, 1, 1, 1); \quad m_2^T = (1, -1, -1, 1, -1, 1, 1, -1);$$

$$m_3^T = (1, -1, 1, -1, 1, -1, 1, -1); \quad m_4^T = (1, -1, 1, -1, -1, 1, -1, 1);$$

$X_i^T = (X_{i1}, X_{i2}, X_{i3}, X_{i4}, X_{i5}, X_{i6}, X_{i7}, X_{i8})$ nodal coordinates

$U_i^T = (U_{i1}, U_{i2}, U_{i3}, U_{i4}, U_{i5}, U_{i6}, U_{i7}, U_{i8})$ nodal displacements

$$U_i^0 = S^T U_i, \quad U_i^{l_1} = l_1^T U_i, \quad U_i^{l_2} = l_2^T U_i, \quad U_i^{l_3} = l_3^T U_i$$

$$U_i^{m_1} = m_1^T U_i, \quad U_i^{m_2} = m_2^T U_i, \quad U_i^{m_3} = m_3^T U_i, \quad U_i^{m_4} = m_4^T U_i$$

The physical meanings of several coefficients in Eq. (4) are interpreted as follows: U_i^0 represents three displacements at the element center accounting for three rigid body translations; $U_i^{l_k}$ represents the constant terms of displacement gradient, and define nine displacement modes: three uniform normal strain modes and six uniform shear strain modes. $U_i^{m_k}$ represents the non-constant terms of displacement gradient, and define twelve hourglass modes: six pure bending modes, three torsion modes and three warping modes. Since the linear independent among S^T , l_i^T and m_j^T :

$$S^T l_i = 0 \quad i = 1, 2, 3 \quad (5)$$

$$S^T m_j = 0 \quad j = 1, 2, 3, 4 \quad (6)$$

$$l_i^T m_j = 0 \quad (7)$$

$$l_i^T l_k = \delta_{ik} \quad k = 1, 2, 3 \quad \delta_{ik} \text{ is Kronecker delta} \quad (8)$$

$$m_n^T m_j = \delta_{nj}, \quad n = 1, 2, 3, 4 \quad (9)$$

Element displacement field could be explained as the linear combination of the above vectors: S^T , l_i^T and m_j^T , in which S^T , l_i^T and m_j^T represent rigid motion, constant deformation modes and spurious deformation modes, respectively. See more information in paper [Li KP and Cescotto S(1997); Wang J and Wagoner RH(2005)].

3 Deformation gradient field and properties of two displacement modes

Only another form of displacement field is given here, with detailed information about deduce process in paper [Li KP and Cescotto S(1997)].

$$u_i = (G_0^T + x_j b_j^T + h_k \gamma_k^T) U_i, \quad j = 1, 2, 3 \quad k = 1, 2, 3, 4 \quad (10)$$

with

$$C = \frac{1}{8} \begin{bmatrix} l_1^T X_1 & l_2^T X_1 & l_3^T X_1 \\ l_1^T X_2 & l_2^T X_2 & l_3^T X_2 \\ l_1^T X_3 & l_2^T X_3 & l_3^T X_3 \end{bmatrix}^{-1} \quad (11)$$

$$b_k = C_{\alpha k} l_k \quad k, \alpha = 1, 2, 3 \quad (12)$$

$$G_0^T = (S - (S^T X_j) b_j)/8 \quad j = 1, 2, 3 \text{ summation on repeated subscript} \quad (13)$$

$$\gamma_k = (m_k - (m_k^T X_j) b_j)/8 \quad j = 1, 2, 3 \quad k = 1, 2, 3, 4 \text{ summation on repeated subscript} \quad (14)$$

$$h_1 = \eta \zeta; \quad h_2 = \xi \zeta; \quad h_3 = \xi \eta; \quad h_4 = \xi \eta \zeta \quad (15)$$

From the above formulations, the following orthogonalities of Eq.s from (16) to (22) are verified:

$$b_i^T X_k = \gamma_{ik} \quad k, i = 1, 2, 3 \quad (16)$$

$$b_i^T S = 0 \quad i = 1, 2, 3 \quad (17)$$

$$b_i^T m_j = 0 \quad i = 1, 2, 3 \text{ and } j = 1, 2, 3, 4 \quad (18)$$

$$S^T m_j = 0 \quad j = 1, 2, 3, 4 \quad (19)$$

$$\gamma_i^T S = 0 \quad i = 1, 2, 3 \quad (20)$$

$$\gamma_i^T m_j = m_i^T m_j = \delta_{ij} \quad i, j = 1, 2, 3, 4 \quad (21)$$

$$\gamma_i^T X_j = 0 \quad i = 1, 2, 3, 4 \text{ and } j = 1, 2, 3 \quad (22)$$

The displacement gradient could be obtained by taking derivatives of Eq. (10)

$$u_{i,j} = \frac{\partial u_i}{\partial x_j} = (b_j^T + h_{k,j} \gamma_k^T) U_i = u_{i,j}^0 + u_{i,j}^h, \text{ summation on repeated subscript} \quad (23)$$

where

$$u_{i,j}^0 = b_j^T U_i; \quad u_{i,j}^h = h_{k,j} \gamma_k^T U_i \quad k = 1, 2, 3, 4, \text{ summation on repeated subscript} \quad (24)$$

It can be observed from Eq. (23) that the displacement gradient is divided into two parts: constant and non-constant part and both of them will be briefed in the following sections.

Arbitrary linear displacement modes of eight nodes

$$U_i = \alpha_i S + \alpha_{ij} X_j \quad (25)$$

According to the orthogonalities of Eqs (16) and (17), we can obtain the following form by substituting Eq. (25) into Eq. (24)

$$u_{i,j}^0 = b_j^T U_i = b_j^T (\alpha_i S + \alpha_{ik} X_k) = \alpha_{ik} b_j^T X_k = \alpha_{ik} \eta_{jk} = \alpha_{ij} \quad (26)$$

According to the orthogonalities of Eqss (20) and (22), one gets

$$u_{i,j}^h = h_{k,j} \gamma_k^T (\alpha_i S + \alpha_{ij} X_j) = 0 \quad (27)$$

Then

$$u_{i,j} = u_{i,j}^h \quad (28)$$

It can be clearly seen that the linear field can be rebuilt when the displacement modes of nodes is linear, and satisfies the consistency condition of element while the hourglass gradient mode vanishes.

Arbitrary hourglass displacement modes of eight nodes:

$$U_i = d_{ij} m_j \quad (29)$$

Considering the orthogonality of Eq. (18), one gets by substituting Eq. (29) into Eq. (24)

$$u_{i,j}^0 = b_j^T d_{ij} m_j = 0 \quad (30)$$

According to the orthogonalities of Eq. (24) and Eq. (21), one can get

$$u_{i,j}^h = h_{k,j} \gamma_k^T (d_{in} m_n) = h_{k,j} d_{in} \gamma_k^T m_n = h_{k,j} d_{in} m_k^T m_n \quad (31)$$

If the displacement modes of nodes are in hourglass modes, those modes have no influence on element's constant strain field. In other words, new 3D element using assumed strain method doesn't damage element's constant strain field, and thus the convergence of new element would be ensured. The building of assumed strain field will be introduced in the following section.

For nonlinear problems, one only needs to replace $(-\sqrt{3}, \sqrt{3}, 0)$, $(-\sqrt{3}, -\sqrt{3}, 0)$ with $(\sqrt{3}, -\sqrt{3}, 0)$, $f^{int} = \int_{\Omega_e} \bar{B} \sigma d\Omega = \sum_{i=1}^n w_i J_i \bar{B}_i \sigma_i$ respectively.

$$\dot{u}_{i,j} = (b_j^T + h_{k,j} \gamma_k^T) \dot{U}_i \quad (32)$$

Noting velocity gradient as

$$\nabla v = \begin{bmatrix} u_{x,x} \\ u_{y,y} \\ u_{z,z} \\ u_{x,y} + u_{y,x} \\ u_{x,z} + u_{z,x} \\ u_{z,y} + u_{y,z} \end{bmatrix} = B \begin{bmatrix} \dot{U}_1 \\ \dot{U}_2 \\ \dot{U}_3 \end{bmatrix} = B\dot{U} \quad (33)$$

where

$$B = \begin{bmatrix} b_1^T + h_{k,1}\gamma_k^T & 0 & 0 \\ 0 & b_2^T + h_{k,2}\gamma_k^T & 0 \\ 0 & 0 & b_3^T + h_{k,3}\gamma_k^T \\ b_2^T + h_{k,2}\gamma_k^T & b_1^T + h_{k,1}\gamma_k^T & 0 \\ b_3^T + h_{k,3}\gamma_k^T & 0 & b_1^T + h_{k,1}\gamma_k^T \\ 0 & b_3^T + h_{k,3}\gamma_k^T & b_2^T + h_{k,2}\gamma_k^T \end{bmatrix}, \quad k = 1, 2, 3, 4,$$

summation on repeated subscript (34)

FI method would lead to volumetric or shear locking, while RI method's main disadvantage is the presence of hourglass modes[Belytschko T, Liu WK and Moran B et al. (2002)]. When the element suffers spurious modes, it would result in zero energy, so such modes are also called zero energy modes. As shown in Eq. (30), it would give rise to twelve hourglass modes because of integration only in the element center.

3.1 Hu-Washizu variational principle

Hu-Washizu variational principle [Fish J and Belytschko T(1998)] for nonlinear problems is expressed as

$$0 = \delta \prod(v, \dot{\bar{\varepsilon}}, \bar{\sigma}) = \int_{\Omega_e} \delta \dot{\bar{\varepsilon}}^T \sigma d\Omega + \int_{\Omega_e} \bar{\sigma}^T (\nabla v - \dot{\bar{\varepsilon}}) d\Omega - \delta \dot{U}^T f^{ext} \quad (35)$$

where δ denotes variation symbol, Ω_e is element domain, v is velocity field, $\dot{\bar{\varepsilon}}$ is interpolated deformation rate, $\bar{\sigma}$ is interpolated stress, σ is stress obtained from the stress-strain law, \dot{U} is velocity of nodes and f^{ext} is external nodal loads. It is necessary to illustrate that the dot above $\dot{\bar{\varepsilon}}$ isn't a meaning of derivative, but a strain variation during an incremental time step.

According to the simplified form of the Hu-Washizu variational principle described by Simo and Hughes (1986), interpolate stress is assumed to be orthogonal to the

difference between the symmetric part of the velocity gradient and the interpolated deformation rate, so Eq. (34) is written as

$$0 = \delta \prod (\dot{\bar{\epsilon}}) = \int_{\Omega_e} \delta \dot{\bar{\epsilon}}^T \sigma d\Omega - \delta \dot{U}^T f^{ext} \quad (36)$$

Obviously, variation principle is independent of the interpolated stress, which doesn't appear in the final equations and needn't to be defined. Now let's define

$$\dot{\bar{\epsilon}} = \bar{B} \begin{bmatrix} \dot{U}_1 \\ \dot{U}_2 \\ \dot{U}_3 \end{bmatrix} = \bar{B} \dot{U} \quad (37)$$

Substituting Eq. (36) into Eq. (35), we get

$$0 = \delta \prod (\dot{\bar{\epsilon}}) = \int_{\Omega_e} \delta \dot{U}^T \bar{B} \sigma d\Omega - \delta \dot{U}^T f^{ext} = \delta \dot{U}^T \left(\int_{\Omega_e} \bar{B} \sigma d\Omega - f^{ext} \right)$$

then

$$f^{int} = f^{ext} \quad (38)$$

where

$$f^{int} = \int_{\Omega_e} \bar{B} \sigma d\Omega \quad (39)$$

Since this dynamic explicit program aims to solve large deformation nonlinear elastic-plastic problems, stress $\sigma = \sigma(\dot{\bar{\epsilon}})$ is related with σ and $\dot{\bar{\epsilon}}$. In order to adapt 3D anisotropic yield criteria and make much more performance on avoiding shear locking, a local coordinate frame is defined, which is embedded in each element and rotates with element [Wang J and Wagoner RH(2005)].

3.2 Assumed velocity strain field

In order to eliminate transverse shear locking or volumetric locking, only non-constant part of B matrix is projected and constant is kept in Belytschko and Binder [7]:

$$B = B_0 + B_\alpha \quad (40)$$

$$\bar{B} = B_0 + \bar{B}_\alpha \quad (41)$$

where

$$B_0 = \begin{bmatrix} b_1^T & 0 & 0 \\ 0 & b_2^T & 0 \\ 0 & 0 & b_3^T \\ b_2^T & b_1^T & 0 \\ b_3^T & 0 & b_1^T \\ 0 & b_3^T & b_2^T \end{bmatrix} \quad B_\alpha = \begin{bmatrix} h_{k,1}\gamma_k^T & 0 & 0 \\ 0 & h_{k,2}\gamma_k^T & 0 \\ 0 & 0 & h_{k,3}\gamma_k^T \\ h_{k,2}\gamma_k^T & h_{k,1}\gamma_k^T & 0 \\ h_{k,3}\gamma_k^T & 0 & h_{k,1}\gamma_k^T \\ 0 & h_{k,3}\gamma_k^T & h_{k,2}\gamma_k^T \end{bmatrix} \quad (42)$$

In order to remove volumetric locking in nearly incompressible or incompressible materials, this program remains the same isochoric field as in WW3D element. There is a little difference from WW3D element in which parts of shear velocity strain are wiped off. Then the expression of the projected B matrix is written as follows

$$\bar{B}_\alpha = \begin{bmatrix} \frac{2}{3}(h_{2,1}\gamma_2^T + h_{3,1}\gamma_3^T + h_{4,1}\gamma_4^T) & -\frac{1}{3}(h_{1,2}\gamma_1^T + h_{3,2}\gamma_3^T + h_{4,2}\gamma_4^T) & -\frac{1}{3}(h_{1,3}\gamma_1^T + h_{2,3}\gamma_3^T + h_{4,3}\gamma_4^T) \\ -\frac{1}{3}(h_{2,1}\gamma_2^T + h_{3,1}\gamma_3^T + h_{4,1}\gamma_4^T) & \frac{2}{3}(h_{1,2}\gamma_1^T + h_{3,2}\gamma_3^T + h_{4,2}\gamma_4^T) & -\frac{1}{3}(h_{1,3}\gamma_1^T + h_{2,3}\gamma_3^T + h_{4,3}\gamma_4^T) \\ -\frac{1}{3}(h_{2,1}\gamma_2^T + h_{3,1}\gamma_3^T + h_{4,1}\gamma_4^T) & -\frac{1}{3}(h_{1,2}\gamma_1^T + h_{3,2}\gamma_3^T + h_{4,2}\gamma_4^T) & \frac{2}{3}(h_{1,3}\gamma_1^T + h_{2,3}\gamma_3^T + h_{4,3}\gamma_4^T) \end{bmatrix} \begin{bmatrix} h_{1,2}\gamma_1^T & h_{2,1}\gamma_2^T & 0 \\ h_{1,3}\gamma_1^T & 0 & h_{3,1}\gamma_3^T \\ 0 & h_{2,3}\gamma_2^T & h_{3,2}\gamma_3^T \end{bmatrix} \quad (43)$$

From the above expression, element meets isochoric everywhere in element which means that element dilatation is zero. The following is the verification.

$$D = \dot{\varepsilon}_x + \dot{\varepsilon}_y + \dot{\varepsilon}_z = b_i^T U_i \text{ summation on repeated subscript} \quad (44)$$

Since element is constant volume, volumetric variation overall element is zero:

$$0 = \int_{\Omega_e} D d\Omega = \int_{\Omega_e} (\dot{\varepsilon}_x + \dot{\varepsilon}_y + \dot{\varepsilon}_z) d\Omega \quad (45)$$

On the use of $\int_{\Omega_e} h_{i,j} d\Omega = 0$, Eqs (36), (40) and (42), Eq. (44) is simplified:

$$\begin{aligned} 0 &= \int_{\Omega_e} (\dot{\varepsilon}_x + \dot{\varepsilon}_y + \dot{\varepsilon}_z) d\Omega \\ &= \int_{\Omega_e} (b_1^T U_1 + b_2^T U_2 + b_3^T U_3) d\Omega = (b_1^T U_1 + b_2^T U_2 + b_3^T U_3) V_e \end{aligned} \quad (46)$$

$$x_i = \sum_{j=1}^8 N_j X_{ij} = (S^T + l_1^T \xi + l_2^T \eta + l_3^T \zeta + m_1^T \eta \zeta + m_2^T \xi \zeta + m_3^T \xi \eta + m_4^T \xi \eta \zeta) X_i / 8$$

denotes the element volume. So Eq. (43) is verified.

Here four-point integration in plane method is applied to evaluated internal force. Those points are located as follows:

$$(\sqrt{3}, \sqrt{3}, 0), \quad (-\sqrt{3}, \sqrt{3}, 0), \quad (-\sqrt{3}, -\sqrt{3}, 0), \quad (\sqrt{3}, -\sqrt{3}, 0)$$

Based on Gauss integration for Eq. (38), we can obtain

$$f^{int} = \int_{\Omega_e} \bar{B} \sigma d\Omega = \sum_{i=1}^n w_i J_i \bar{B}_i \sigma_i \quad (47)$$

where n denotes the number of integration points, and w_i , J_i , \bar{B}_i , σ_i denote the weight coefficient of i th point, determinant of Jacobian matrix, l_3^T matrix and stress vectors respectively. Generally, weight coefficients are set to be 2 for four-point integration. The choice of integration points is a little different from other references, and we choose four points in plane and multiple layers along thickness direction to detect stress and strain states in transversal and thickness direction.

The return mapping algorithm, 3D anisotropic yield criteria and adaptive mesh refine algorithm are ignored here due to the length of a journal paper.

4 Simulation examples

Considering the limit of dynamic explicit method, this program is suitable for dynamic or quasi-static problems. So examples about static couldn't be executed. One bending simulation of thick metal and two bulk forming examples are implemented.

4.1 Thick plate bending

As shown in Fig. 2, sheet's geometry for this problem is: length $L=50\text{mm}$, width $w=10\text{mm}$, thickness $H=10\text{mm}$, punch radius $R1=23.5\text{mm}$, die radius $R2=25\text{mm}$, die round radius $R3=4\text{mm}$. Other parameters are setting: punch stroke $H=14\text{mm}$, punch speed $v=6\text{m/s}$.

The material is normal steel, which obey the hardening curve $\sigma = 600(0.001 + \varepsilon)^{0.22}$ MPa, and Young's modulus $E=207\text{G Pa}$, Poisson's ratio $\nu=0.3$, friction coefficient among contact surfaces $\mu=0.1$, Yield stress $\sigma_y = 200\text{MPa}$.

It is well-known that it is apt to stimulate hourglass modes in point or line contact. According to the experience of the solid-shell element application in sheet metal forming, the more contact is between blank and dies, the harder the occurrence of hourglass will be. With the punch moving downward, it is a line contact at the beginning, which is subject to active hourglass modes. From the deformed mesh in Fig. 3, we could see that spurious modes are under control. In the next part,

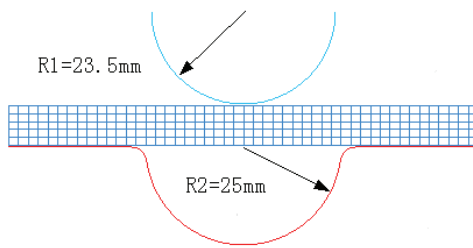


Figure 2: Finite element mode of thick plate

the author makes a detailed comparison of new element with four-point integration ADS and ASQBI element (Belytschko T and Bindeman LP, 1993) on the basis of dynamic explicit method.

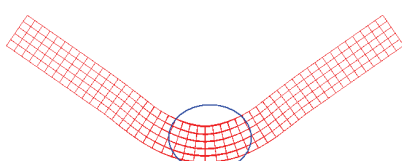


Figure 3: Deformed result of new solid in front view

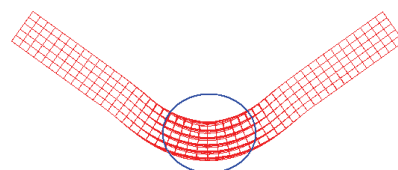


Figure 4: Deformed result of ASQBI solid in front view

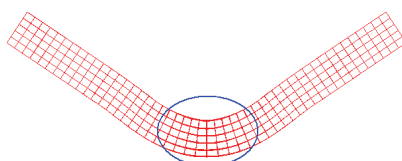


Figure 5: Deformed result of ADS solid in front view

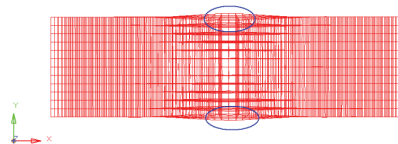


Figure 6: Deformed result of ASQBI solid in top view

Fig. 3, Fig. 4 and Fig. 5 are the front views showing the deformed results of new solid, ASQBI and ADS respectively. As mentioned in reference [Belytschko T and Bindeman LP(1993)], ADS element performs better than ASQBI in elastic-plastic bending problems, which is verified in Fig. 4 and Fig. 5. In the Y direction of sections between thick plate and punch, especially in the edge parts, ASQBI element overstates the deformation as is shown in Fig. 6, while ADS element and

new element is much closer, as is shown in Fig. 3 and Fig. 5. The Expression of the new solid element's $\sigma = 600(0.001 + \varepsilon)^{0.22}$ is close to that of ADS's which is equivalent to the deviatoric part of $\sigma_y = 200$, so new solid element could describe the deformation of elastic-plastic materials as ADS element. The load-stroke relations using above solid elements are given in Fig. 7. As we can see, the curve of new element is much closer to that of the ADS element.

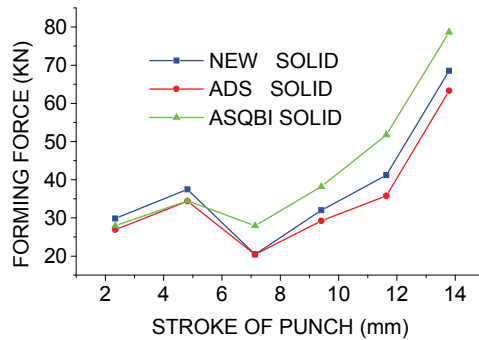


Figure 7: Comparison of three solid elements

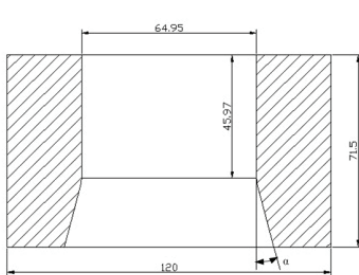


Figure 8: Ironing die

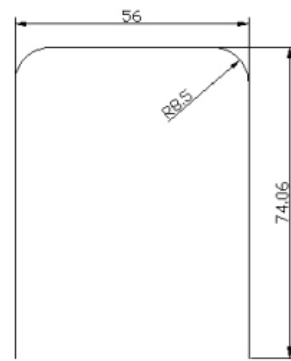


Figure 9: Ironing punch

4.2 Thick metal plate ironing

The section view in Fig. 8 illustrates the dimension of the ironing die. The die consists of a semi angle $\alpha = 10.2^\circ$, arc curve R8 and a straight-line segment. Fig. 9

shows the dimension of ironing punch. The round $R8.5$ of punch can prevent stress concentration. Fig. 10 illustrates the dimension of initial semi-finished product with X_{i7} as its initial wall thickness and $T_f = 4.475$ mm as the final thickness. The punch stroke is 35mm. Four layer solid elements along thickness direction are meshed for product and quadrangle meshes are for ironing die and punch.

The material used in this problem is normal steel, obeying the following hardening curve $\sigma = 80.3944(0.0151 + \bar{\varepsilon}_p)^{0.33944} \text{kgf / mm}^2$, Young's modulus U_{i6} , Poisson's ratio $\nu=0.3$, $1\text{kgf} = 9.81\text{N}$, Yield stress $\sigma_y = 19.4\text{kgf / mm}^2$. See more information in reference (Huang YM, Lu YH and Chan JW, 1991).

After defining ironing coefficient $R = T_i/T_f$, choosing $\alpha = 10.2^\circ$, friction $\mu = 0.03$, and giving two teams of ironing coefficient $R = 1.4$, U_{i1} , one gets two teams of load-stroke relations shown in Fig. 11 and Fig.12 respectively. The relation between stroke and forming force is much coincident with experimental results in reference [Huang YM, Lu YH and Chan JW (1991)]. The occurrence of polygonal line of simulation data is of the out and in around the die angle of the product nodes alternatively. The force increases with the stroke of punch and keeps stable when the stroke is up to a certain value theoretically.

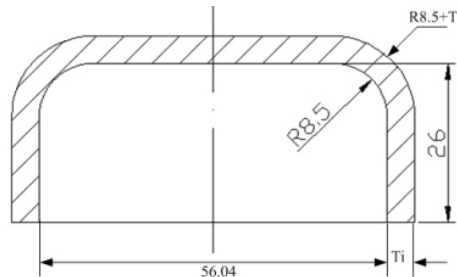


Figure 10: Semi-finished products

With the movement of punch, the materials begin to enter the die and are squeezed. Meanwhile, the force increases correspondingly, as is shown in Fig. 13. When materials touch die completely in the angle, the force keeps no variation, as is shown in Fig. 14. After the materials in die angle begin to decrease, the force decreases, as is shown in Fig. 15. It could be deduced that the length of the interval in which the force is constant in term of the constant volume of materials before and after deformation:

$$b = \alpha * R \quad (48)$$

where U_{i3} denotes the wall length shown in Fig. 14. R is the corresponding ironing

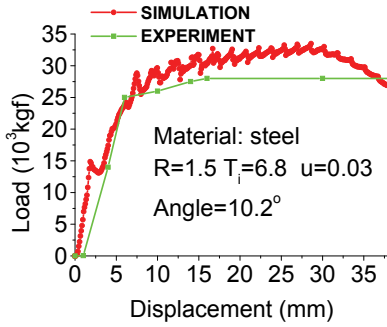


Figure 11: The load-stroke relation with $R=1.5$

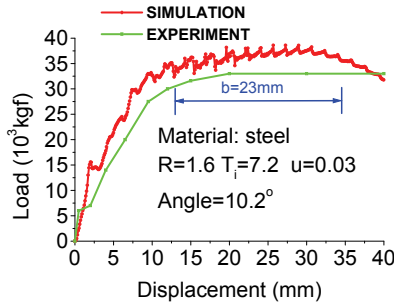


Figure 12: The load-stroke relation with $R=1.6$

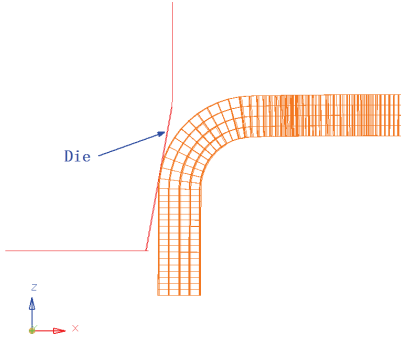


Figure 13: Initial touch of product and die

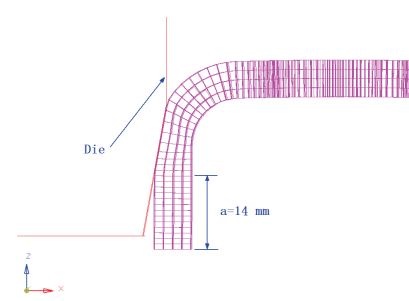


Figure 14: Complete touch of product and die

coefficient. It could be verified that $b = \alpha R = 14 * 1.6 = 22.4\text{mm}$ from Fig. 12.

4.3 Cylindrical piece embossing

Fig. 16 and Fig.17 illustrate the embossing top die and bottom die, respectively. The radius of cylindrical piece is 6 mm and its height is 1.6 mm. Five layer solid elements along thickness are meshed with initial elements number 30810 and nodes number 37410 and adaptive mesh refine three degrades is used because of the high accuracy demanded by client, Shenyang Mint in China. The bottom die is fixed and the top die's total movement is only 0.15 mm, so the deformation of piece is relatively small.

The material used in this example is normal steel, which obeys the hardening curve $\sigma = K(\varepsilon_0 + \varepsilon)^n$ MPa in which the strengthen coefficient $K= 587$, initial strain $\varepsilon_0 =$

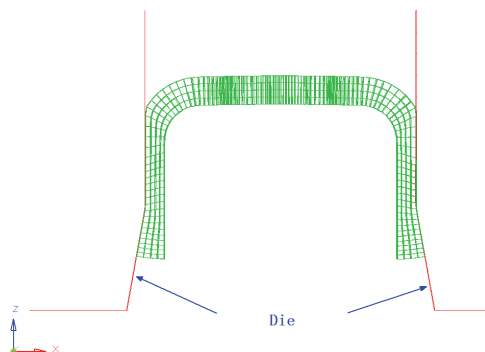


Figure 15: Material in the die decrease



Figure 16: Top die

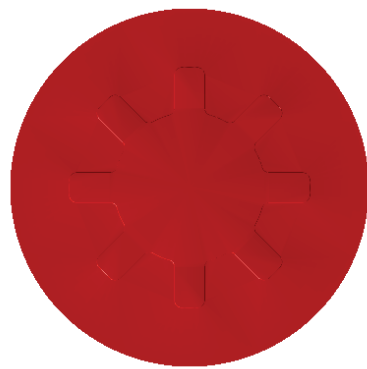


Figure 17: Bottom die

0.001, and harden coefficient $n = 0.27$. Young's modulus $E = 207\text{G Pa}$, Poisson's ratio $\nu = 0.3$, friction coefficient among contact surfaces $\mu = 0.08$, Yield stress $\sigma_y = 200\text{MPa}$.

Fig. 18 shows the deformed result of embossing, and the CPU time is 1 hours. In the region of printed letters and relatively large deformation of the coin, the deformed meshes are depicted considerably clear. It can be seen that there is no hourglass (no mesh picture is given due to the large number of meshes). Of course, the adaptive mesh refine and small deformation are some factors. Figs. 19 and 20 are the strain contour and stress contour of the first layer solid elements respectively.

The above embossing process is also implemented in DEFORM 3D software. Piece is meshed with tetrahedral element, and the element number is setting to be 185739.



Figure 18: Deformed simulation result



Figure 19: Effective strain contour of the first layer elements



Figure 20: Effective stress contour of the first layer elements



Figure 21: Simulation result of DEFORM 3D

All the parameters setting is the same as the new solid element excepting the hardening curve. The whole CPU time is 5.5 hours, and the simulation result is shown

in Fig. 21.

By comparing Fig. 18 with Fig. 21, it is found that the result of new element is much excellent than that of DEFORM 3D. On one hand, the number of tetrahedral element is limited in DEFORM 3D, so tiny characteristics of the piece couldn't be described clearly. On the other hand, 5 layers elements though thickness direction and precise calculation of internal forces, stress and strain using four-point, could represent the elastic-plastic state of the material.

5 Conclusions

The new solid element with four-point integration in plane and assumed strain technology successfully removes locking problems theoretically, and the simulation results of above examples verify that the hourglass modes can be deleted successfully. It is predicted that this new solid element could be widely applied in bulk forming simulation with the continuous improvement of computer performance. The new element is characterized by the following features:

- No volumetric locking because of the usage of assumed strain method.
- No hourglass modes, good performance in bending, for instance, as is shown in case 1.
- No extra computation on anti-hourglass force, and no user-defined parameters.
- Multi-layer elements in thickness, four-point integration, return mapping algorithm, 3D constructive law , double side contact algorithm and adaptive mesh refine technology make the new solid element exhibit excellent advantage in solving lager deformation elastic-plastic problems. Ironing and embossing example demonstrate the accuracy of such element in bulk forming simulation.
- Compared with WW3D element, the computational cost of the new element is reduced by nearly fifth percents.

The paper presents the application of a new solid element in bulk forming simulation, and the results turn out to be effective. However, the volumetric locking of the element is not verified. Therefore, much more work should be devoted to the development of corresponding implicit algorithm to verify the locking problems of this solid element.

Acknowledgement: The work described in this paper is supported by a grant from Special Foundation of Basic R&D for Central College of China (Q2009010), National Key Technology R&D Program (No. 2006BAF01A43). The authors also give their gratitude to senior engineer Li and Hu of Shenyang Mint for their tool models.

References

- Atluri, S. N.; Zhu, T. (1998): A new meshless local Petrov-Galerkin (MLPG) approach in computational mechanics, *Computational Mechanics*, vol. 22, no. 5, pp. 117-127.**
- Atluri S. N.; Shen S. P. (2002): The meshless local Petrov-Galerkin (MLPG) method: A simple & less-costly alternative to the finite element and boundary element methods, *CMES: Computer Modeling in Engineering and Sciences*, vol. 3, no. 1, pp. 11-51**
- Atluri, S. N. (2004): The Meshless Local Petrov-Galerkin (MLPG) Method for Domain & Boundary Discretizations, Tech Science Press.**
- Atluri, S. N.; Han, Z. D.; Rajendran, A. M. (2004): A New Implementation of the Meshless Finite Volume Method, Through the MLPG “Mixed” Approach, *CMES: Computer Modeling in Engineering and Sciences*, vol. 6, No. 6, pp. 491-514**
- Han, Z. D.; Rajendran, A. M.; Atluri, S. N. (2005): Meshless Local Petrov-Galerkin (MLPG) Approaches for Solving Nonlinear Problems with Large Deformations and Rotations, *CMES: Computer Modeling in Engineering and Sciences*, vol. 10, No. 1, pp. 1-12**
- Atluri, S. N.; Liu, H. T.; Han, Z. D. (2006): Meshless Local Petrov-Galerkin (MLPG) Mixed Finite Difference Method for Solid Mechanics, *CMES: Computer Modeling in Engineering and Sciences*, vol. 15, No. 1, pp. 1-16**
- Basar, Y.; Kintzel, O. (2003): Finite rotations and large strains in finite element shell analysis, *CMES: Computer Modeling in Engineering & Sciences*, vol. 4, no. 2, pp. 217-230.**
- Belytschko, T.; Liu, W. K.; Moran, B. (2002): Nonlinear Finite Elements for Continua and Structures. Beijing, China, Tsinghua University Press.**
- Belytschko, T.; Ong, J. S. J; Liu, W. K.; Kennedy, J. M. (1984): Hourglass control in linear and nonlinear problems, *Comp Methods Appl Mech Eng*, vol. 43, no. 2, pp. 251-276.**
- Belytschko, T.; Bindeman, L. P. (1993): Assumed strain stabilization of the eight-node hexahedral element, *Comp Methods Appl Mech Eng*, vol. 105, no. 2, pp.**

225-260.

Cui, X.Y.; Liu, G. R.; Li, G. Y.; Zhao, X.; Nguyen, T.T.; Sun, G.Y. (2008): A smoothed finite element method (SFEM) for linear and geometrically nonlinear analysis of plates and shells, *CMES: Computer Modeling in Engineering & Sciences*, vol.28, no.2, pp. 109-125.

Fish, J.; Belytschko, T. (1998): Elements with Embedded Localization Zones for Large Deformation Problems, *Computers and Structures* , vol. 30, no. 1, pp. 247-256.

Filho, L. A. D.; Awruch, A. M. (2004): Geometrically nonlinear static and dynamic analysis of shells and plates using the eight-node hexahedral element with one-point integration, *Finite Element in Analysis and Design*, **vol. 40**, no. 11, pp. 1297-1335.

Flanagan, D. P.; Belytschko, T. (1981): A uniform strain hexahedron and quadrilateral with orthogonal hourglass control, *Int J Num Methods Eng* , **vol. 17**, no. 5, pp. 679-706.

Fredriksson, M.; Ottosen, N. S. (2007): Accurate eight-node hexahedral element, *Int J Num Methods Eng*, vol. 72, no. 6, pp. 631-657.

Gato, C.; Shie Y. (2008): Numerical Simulations of Dynamic Fracture in Thin Shell Structures, *CMES: Computer Modeling in Engineering & Sciences*, vol. 33, no. 3, pp. 269-292.

Gu, Y. T.; Liu, G. R. (2001): A Meshless Local Petrov-Galerkin (MLPG) Formulation for Static and Free Vibration Analyses of Thin Plates, *CMES: Computer Modeling in Engineering and Sciences*, vol. 2, no. 4, pp. 463-476.

Han, Z. D.; Liu, H. T.; Rajendran, A. M.; Atluri, S. N. (2006): The Applications of Meshless Local Petrov-Galerkin (MLPG) Approaches in High-Speed Impact, Penetration and Perforation Problems, *CMES: Computer Modeling in Engineering and Sciences*, vol. 14, no. 2, pp. 119-128.

Hu, Y. K.; Nagy, L. I. (1997): A one-point integration eight-node brick element with hourglass control, *Computer & Structure*, vol. 65, no. 6, pp. 893-902.

Huang, Y. M.; Lu, Y. H.; Chan, J. W. (1991): An elastic-plastic finite element and experimental study of the ironing process, *J Mater Process Technol*, vol. 26, no. 1, pp. 53-80.

Jarak, T.; Sori, C. J.; Hostler, J. (2007): Analysis of Shell Deformation Responses by the Meshless Local Petrov-Galerkin (MLPG) Approach, *CMES: Computer Modeling in Engineering and Sciences*, vol. 18, no. 3, pp. 235-246.

Jarak, J.; Sori, C. J. (2008): Analysis of rectangular square plates by the mixed Meshless Local Petrov-Galerkin (MLPG) approach, *CMES: Computer Modeling*

in *Engineering and Sciences*, vol. 38, no. 3, pp. 231-262.

Koh, B. C.; Kikuchi, N. (1987): New improved hourglass control for bilinear and trilinear elements in anisotropic linear elasticity, *Comp Methods Appl Mech Eng*, vol. 65, no. 1, pp. 1-46.

Kosloff, D; Frazier, G. A. (1978): Treatment of hourglass patterns in low order finite elements codes, *Int J Num Anal Methods Geomech*, vol.2, no. 1, pp. 57-72.

Kulikov1, G. M.; Plotnikova, S. V. (2008): Finite Rotation Geometrically Exact Four-Node Solid-Shell Element with Seven Displacement Degrees of Freedom, *CMES: Computer Modeling in Engineering&Sciences*, vol. 28, no.1, pp. 15-38.

Lee, K.; Cho, C.; Lee, S. W. (2002): A geometrically nonlinear nine-node solid shell element formulation with reduced sensitivity to mesh distortion, *CMES: Computer Modeling in Engineering& Sciences*, vol. 3, no. 3, pp. 339-349.

Li, K. P.; Cescotto, S. (1997): An 8-node brick element with mixed formulation for large deformation analysis, *Comp Methods Appl Mech Eng*, vol. 141, no. 1-2, pp. 157-204.

Liu, W. K; Ong, J. S. J.; Uras, R. A. (1985): Finite element stabilization matrices-a unification approach, *Comp Methods Appl Mech Eng*, vol. 53, no. 1, pp. 13-46.

Liu, W. K.; Hu, Y. K.; Belytschko, T. (1994): Multiple integration under-integrated finite elements, *Int J Num Methods Eng*, vol. 37, no. 19, pp. 3263-3289.

Liu, W. K.; Guo, Y.; Tang, S.; (1998): A Multiple-integration eight-node hexahedral finite element for large deformation elasto-plastic analysis, *Comp Methods Appl Mech Eng*, vol. 154, no. 1-2, pp. 69-132.

Li, Q.; Shen, S.; Han, Z. D.; Atluri, S. N. (2003): Application of Meshless Local Petrov-Galerkin (MLPG) to Problems with Singularities, and Material Discontinuities, in 3-D Elasticity, *CMES: Computer Modeling in Engineering and Sciences*, vol. 4, no. 5, pp. 571-586.

Long, S. Y.; Atluri, S. N. (2002): A Meshless Local Petrov-Galerkin Method for Solving the Bending Problem of a Thin Plate, *CMES: Computer Modeling in Engineering and Sciences*, vol. 3, no. 1, pp. 53-64.

Sori, C, J.; Li, Q.; Jarak, T.; Atluri, S. N. (2004): Meshless Local Petrov-Galerkin (MLPG) Formulation for Analysis of Thick Plates, *CMES: Computer Modeling in Engineering and Sciences*, vol. 6, no. 4, pp. 349-358.

Strang, G. (1972): Variation crimes in the finite element method, in *The Mathematical Foundations of the Finite Element Method with Applications to Partial Differential Equations* (ed. AK Aziz), Academic Press, New York, pp. 689-710.

Wang, J.; Wagoner, R. H. (2005): A practical large-strain solid finite element for sheet forming, *Int J Num Methods Eng*, vol. 63, no. 4, pp. 473-501.

Simo, J. C.; Hughes, T. J. R. (1986): On the variation foundations of assumed strain methods, *J Appl Mech*, vol. 53, no. pp. 51-54.